Check for updates

Research Article

Adsorption Science & Technology
Volume 43: 1–21
© The Author(s) 2025
Article reuse guidelines:
sagepub.com/journals-permissions
DOI: 10.1177/02636174251314596
journals.sagepub.com/home/adt
Sage

Incorporation of active phases of iron and bone char in clay ceramic monolith for arsenic removal from aqueous solutions

Celene García-Carvajal
Laboratorio de Sólidos Porosos, INFAP-CONICET, Universidad Nacional de San Luis, San Luis, Argentina
Facultad de Química, Bioquímica y Farmacia, Universidad Nacional de San Luis, San Luis, Argentina

Jhonny Villarroel-Rocha
Laboratorio de Sólidos Porosos, INFAP-CONICET, Universidad Nacional de San Luis, San Luis, Argentina

Didilia Ileana Mendoza-Castillo
Laboratorio de Ingeniería y Tecnología del Agua, Instituto Tecnológico de Aguascalientes, Aguascalientes, México

Adrián Bonilla-Petriciolet
Laboratorio de Ingeniería y Tecnología del Agua, Instituto Tecnológico de Aguascalientes, Aguascalientes, México

Karim Sapag
Laboratorio de Sólidos Porosos, INFAP-CONICET, Universidad Nacional de San Luis, San Luis, Argentina

Abstract

Clay-based monoliths with incorporation of active phases derived from the waste of the metallurgical and livestock industries (powdered iron and bone meal) and composite with both raw

Corresponding authors:
Jhonny Villarroel-Rocha, Laboratorio de Sólidos Porosos, INFAP-CONICET, Universidad Nacional de San Luis, Avenida Ejército de los Andes 950 – CP: 5700, San Luis, Argentina.
Email: jhoviro@gmail.com

Karim Sapag, Laboratorio de Ingeniería y Tecnología del Agua, Instituto Tecnológico de Aguascalientes, C.P. 20256 Aguascalientes, México.
Email: sapag@unsl.edu.ar

Creative Commons CC BY: This article is distributed under the terms of the Creative Commons Attribution 4.0 License (https://creativecommons.org/licenses/by/4.0/) which permits any use, reproduction and distribution of the work without further permission provided the original work is attributed as specified on the SAGE and Open Access page (https://us.sagepub.com/en-us/nam/open-access-at-sage).

materials were synthesized by the extrusion process and used as adsorbents in the As(V) removal from aqueous solutions. These monoliths exhibited excellent mechanical properties compared to commercial ceramic-based monoliths, with potential for their use in continuous systems due to ease of handling and extraction of the adsorption medium (i.e., packed bed) and having defined meso and macroporosity. Specifically, the clay-based monoliths were obtained along with (i) active iron phases (hematite and magnetite), (ii) bone char and (iii) a combination of both materials. They showed As(V) adsorption capacities of up to 0.56, 3.4 and 8.0 mg g^{-1} at neutral pH and room temperature conditions. The proposed adsorption mechanism was associated with ligand exchange between the As(V) species and the hydroxyl functional groups, in addition to the presence of inner-sphere bidentate unprotonated arsenate surface complexes that was reflected in the formation of new absorption bands in Fourier Transform Infrared Spectroscopy spectra related to the Metal-O interaction and changes in the bands associated with the -OH groups. The SIPS isotherm model fitted the experimental data obtained at equilibrium and was related to strong adsorbent/adsorbate interactions and high surface heterogeneity. Finally, the composite ceramic monolith synthesized in the present study exhibits capabilities comparable to those reported in the literature, highlighting the low cost of raw materials, as well as its excellent mechanical properties and well-defined porosity.

Keywords
water decontamination, geogenic depollution, clay ceramic monolith, iron, bone char, arsenic removal

Introduction

According to the World Health Organization, arsenic (As) is a naturally occurring metalloid in the environment, ranked as one of the ten chemicals of most significant concern to public health. This element is abundant in several world regions, mainly in Bangladesh, Argentina, the United States, India, Germany, China, Spain, Mexico, Canada, New Zealand and Thailand (Altowayti et al., 2022). Water contaminated with arsenic is a severe problem for public health, especially in regions where groundwater is used as the primary source for human consumption.

Continuous exposure to As via drinking water is the main cause of some severe diseases due to its toxic and carcinogenic potential, especially Chronic Regional Endemic Hydroarsenicism, a disease caused by the systematic consumption of water contaminated with more than 10 μg As L^{-1}, which is characterized by skin lesions and cancerous and non-cancerous systemic alterations (Alka et al., 2021; Litter, 2010). In addition, the toxicology of this environmental pollutant has been associated with the incidence of cardiovascular diseases and neurological problems, among other adverse effects (Costa et al., 2024). Various treatment technologies have been developed to face As water pollution (Singh et al., 2021), with adsorption being one of the most effective and widely studied methods, not only because competitive removal results are obtained in its application but also because a wide range of adsorbent materials with suitable physicochemical properties for each pollutant can be used (Altowayti et al., 2022; Hao et al., 2018; Srivastav et al., 2022). In particular, the adsorbents developed from low-cost natural materials make this process a feasible and economical technology compared to other water purification methods (Mohanty, 2017).

There are a variety of studies reported for the arsenic removal in aqueous media, including biosorbents, carbon-based adsorbents, nano-compounds, zeolites, minerals, MOFs, among others, which supports the great diversity of materials developed for this application (Alka et al., 2021; Altowayti et al., 2022;

Sharma et al., 2022; Srivastav et al., 2022; Weerasundara et al., 2021).

Among the low-cost natural materials that have been most researched for the arsenic removal present in water are natural clays (Baigorria et al., 2021; Mukhopadhyay et al., 2021), and among them, the best results found in the literature are for: (i) montmorillonite with As(V) removal capacities between 0.04 and 0.64 mg g^{-1} (Mohapatra et al., 2007; Te et al., 2017); (ii) illite with a maximum As(V) removal capacity of 0.52 mg g^{-1} (Mohapatra et al., 2007); and (iii) kaolinite with As(V) removal capacities between 0.23 and 0.86 mg g^{-1} (Ladeira & Ciminelli, 2004). These clays can remove As thanks to the fact that their sheets have edge sites, which are the hydroxyl terminal groups of the silanol (Si-OH) and aluminol (Al-OH) groups (Liu et al., 2014). They are the only surface hydroxyl groups (-OH) that can exchange protons with the medium, making the surface charge of these clays pH-dependent. Edge sites in clays become positively charged at acidic pH, resulting in these groups having a higher affinity for anionic species, such as arsenate and arsenite anions. This explains why the arsenic adsorption capacity of montmorillonites increases at a pH below 7 (García-Carvajal et al., 2019).

On the other hand, iron is one of the most efficient active elements for removing arsenic from aqueous solutions (both mass-borne and supported and in different phases) (Gong et al., 2023; Gu et al., 2007; Huo et al., 2017; Lafferty & Loeppert, 2005; Rha et al., 2019; Sylvester et al., 2007; Weerasundara et al., 2021; Zhu et al., 2009) since arsenic has a great electrostatic attraction for iron-based adsorption sites, where some of the proposed mechanisms are: in hydrated iron oxide through exchange with OH groups (Huo et al., 2017) and in iron oxyhydroxides (FeOOH) that behave as positive colloids, where anion adsorption occurs forming complex anions, where arsenate and arsenite constitute mono- and bidentate complexes with goethite (α-FeOOH) (Farrell & Chaudhary, 2013; Huo et al., 2017). Additionally, iron is attractive for arsenic removal due to its high adsorption capacity, which can vary from 0.05 to 153.8 mg g^{-1} (Gong et al., 2023; Hao et al., 2018), availability, low cost as well as its ease of preparation and compatibility with other water treatment processes.

Other low-cost materials studied in arsenic removal are hydroxyapatite and calcite, minerals found naturally in animal bones. Here, phosphates and carbonates in bone meal can be crucial in removing arsenic from water. Phosphates can form complexes with arsenic and help to adsorb or precipitate it, while carbonates can influence the pH of water and the interactions between arsenic and bone meal. These mineral components make the bone meal a potentially effective option for arsenic removal from water, specifically, with this type of material, As(V) removal capacities were found between 0.34 and 4.5 mg g^{-1} (Alkurdi et al., 2021; Brunson & Sabatini, 2009; Chen et al., 2008; Hao et al., 2018; Sneddon et al., 2005).

Herein, it is essential to emphasize that a primary disadvantage of these materials is their use in powdered form. When clays come into contact with water, their laminar structure exhibits swelling, complicating their extraction from the aqueous medium. This issue is similar to extracting iron powder and animal bone meal powder from liquids. A viable solution to this challenge is the utilization of conformal adsorbents in appropriate structural forms, such as monoliths, extruded pellets or three-dimensional structures (Villarroel-Rocha, 2012). An alternative to keeping these structures stable is to develop them as ceramic structures, which stand out for having high mechanical strength, uniform porosity and low-pressure drop, and therefore, they are useful to avoid plugging in the operation of packed bed columns (Avila et al., 2005).

Therefore, the present work shows the results obtained in the synthesis and characterization of ceramic monoliths based on natural clays with activated phases given by the incorporation of iron powder (CM_Fe), carbonized

bone (CM_BC) and a composite with both active phases (CM_BC@Fe). These materials were applied to remove arsenic in water, emphasizing the characterization of their physicochemical properties and use in the form of monoliths.

Materials and methods

Preparation of ceramic monoliths

Ceramic monoliths were obtained using the synthesis conditions reported by (García-Carvajal et al., 2019) as the following:

1. *Obtaining ceramic paste:* Bone meal from the Bolivian company 'Vital' and iron powder as waste from the Argentinian metallurgical company 'Kieva Industrial' were used as active phases. Bentonitic clay, donated by the company 'Santa Gema' from San Juan, Argentina, was used as a plasticizer and provided ceramic body. The chemical compositions of these raw materials are presented in Tables 1 and 2. Commercial starch and carboxymethylcellulose were used as binders. The ceramic paste is obtained from a mixture of the previously sifted raw materials, according to the proportion indicated in Table 3. The raw materials were placed in a horizontal mixer at 60 rpm for 15 min to ensure the homogeneity of the mixture, and approximately 30–35% w/w of water was added to obtain a paste with the necessary rheology so that it could pass through the nozzle and achieve the final geometry.
2. *Extrusion:* At this stage, the green ceramic paste with the appropriate rheological properties was initially passed through the feed hopper to a simple geometry nozzle to deaerate and homogenize the paste completely, then the nozzle was changed, and 20 cm long × 2.7 cm wide honeycomb monoliths were obtained with 2 mm × 2 mm cells and 0.9 mm thick walls.
3. *Drying and heat treatment:* In this last stage, once extruded, the materials were taken to a vacuum chamber at room temperature for 48 h, ensuring a slow drying to avoid breakage and deformation in the monolith structure due to the rapid evaporation of water. They were then taken to a furnace where heat treatment was carried out with a heating ramp of 5 °C min^{-1} from room temperature to the final calcination temperature as appropriate for 1 h.

It was previously found that, in the case of ceramic monoliths containing bone meal, the one with a 50% active phase and carbonized in an inert atmosphere (N_2) at 700 °C exhibited the best adsorptive properties. In contrast, the monoliths containing iron powder with the best adsorptive and mechanical properties were those with 25% active phase and calcined in air at 600 °C. The clay content in the monoliths was adjusted according to the active phase proportion, while consistently maintaining 5% binder in the final composition for all formulations. A summary of the synthesis conditions for each ceramic monolith is presented in Table 3.

Characterization of raw materials and ceramic monoliths

X-ray diffraction (XRD), X-Ray fluorescence, Fourier Transform Infrared Spectroscopy (FTIR), scanning electron microscopy (SEM), mercury porosimetry and axial compression test were used for determining the physicochemical properties and characteristics of surface chemistry of raw materials and ceramic monoliths with Fe and bone char.

The crystalline structures of adsorbents were analyzed using an X-ray diffractometer Bruker D8-Advance with mirror Göebel that has a

Table 1. Chemical composition of bentonite and bone meal (expressed as oxides).

Bentonite clay (%)		Bone meal (%)	
Fe_2O_3	1.7	Fe_2O_3	0.2
K_2O	0.5	K_2O	0.4
CaO	1.3	CaO	30.7
SiO_2	60.2	SiO_2	6.2
TiO_2	0.3	TiO_2	0.04
Al_2O_3	13	Al_2O_3	1.3
MgO	11.6	MgO	3.5
P_2O_5	0	P_2O_5	15.7
CL*	10.7	CL*	40.6

*Calcination losses at 1000°C.

Table 2. Semi-quantitative analysis of the iron phases present in iron powder.

Iron phases (%)*	
Fe_3O_4 (Magnetite)	51
Fe_2O_3 (Hematite)	49

*Amounts calculated by RIR (Reference Intensity Ratio) method by XRD.

tube with cooper anode RX and Cu Kα ($\lambda =$ 0.15406 nm) radiation. The diffractograms were obtained in a range of $10° \leq 2\theta \leq 80°$. The identification of the mineralogical phases present in each material, as well as the semi-quantitative analysis of the iron phases using the Reference Intensity Ratio method, were both conducted using the XRD database within the Match software (from Crystal Impact).

Chemical compositions of raw materials were quantified using a Philips X-ray fluorescence spectrometer PW1400, where the powder samples were prepared in the form of pills, the X-ray source was an Rh tube that operated at 50 kV and 50 mA, and the elements analyzed were Fe, K, Ca, Ti, Si, Al, P and Mg, with their respective calibration curves that had at least five patterns.

Functional groups were identified using an FTIR spectrum recorded on a Bruker IFS 66/S spectrophotometer. All samples were analyzed with spectroscopic grade KBr, where 200 scans and a resolution of 4 cm^{-1} were used.

The SEM images presented in this work were obtained with an LEO 1450VP scanning electron microscope. Before analysis, the samples were metallized with a thin film of gold (~10 nm) to ensure sufficient conductivity in the samples and to prevent the surface from being charged with electrons. The images were processed using the open-access Inkscape program.

Textural properties were measured on a porosimeter analyzer, AUTOPORE III (Micromeritics), from 0.002 up to 200 MPa. The samples previously were degassed to a residual pressure of 30 μm Hg. From mercury intrusion data, specific surface area (S_{Hg}), total pore volume (V_{TP}), porosity and pore size distribution were obtained.

To determine the point of zero charge (PZC), the salt addition method (Mustafa et al., 2002) was employed, which involves measuring the pH variation of solutions in contact with a solid sample. The procedure was conducted as follows: 25 mL of a 1.0 M $NaNO_3$ solution was prepared, and the pH of these solutions was adjusted using NaOH and HNO_3 across a range of 1–12. The initial pH was then measured using an OHAUS pH meter equipped with a glass electrode. Following this, 1 g of the ceramic monolith (CM) was added, and the mixture was stirred at 200 rpm on an orbital shaker for 24 h. After this period, the final pH was measured and recorded. The values were subsequently plotted as $\Delta pH =$ final pH – initial pH against the initial pH.

Chemical resistance of the materials was assessed through stability tests in an aqueous medium at various pH levels. Approximately 1.5–2 g of the composite monolith was placed in contact with 0.1 M HCl solution to achieve a pH of ~3, 0.1 M NaOH solution for a pH of ~12, and deionized water for a pH of ~7. Following 24 h of exposure, the material was dried in an oven at 60 °C, and the initial mass was compared to the final mass to determine mass losses due to leaching at the different pH levels.

Table 3. Synthesis parameters of ceramic monoliths obtained from bone char and iron powder.

	Bone char ceramic monoliths (CM_BC)	Iron ceramic monoliths (CM_Fe)	Composite CM (CM_BC@Fe)
Active phase	Bone meal 50% ± 50% ± 0.7%	0.6% ± 0.3%	Iron powder 25% ± bone meal 25% ±
Iron powder	25% ± 0.3%		
Plasticizer and ceramic structure 0.9%	Bentonite clay 45% ± Bentonite clay 20% ±	0.5% 0.3%	Bentonite clay 70% ±
Binder 0.1%	Carboxymethylcellulose 5% ± Carboxymethylcellulose 5% ±	0.1% 0.1%	Starch 5% ±
Heat treatment atmospheres	N_2	Air	N_2
Final carbonization/ calcination temperature	700 °C	600 °C	700 °C

Monolith mechanical properties were obtained with axial compression tests (extrusion direction) using an equipment COMTEN INDUSTRIES 94 V series at a constant speed of 0.01 mm s^{-1}. The data obtained on distance travelled and pressure applied to each ceramic piece was normalized to find deformation (in terms of percentage) and compressive stress (in terms of force per unit area). The modulus of elasticity (Young's modulus) was obtained as the slope of the linear zone of the graph Stress (σ_c) vs. Deformation (ϵ) of each of the materials (García-Carvajal, 2019).

As(V) Adsorption Tests

For adsorption kinetics, a fixed mass of 6 g of monolith was taken in a volume of 500 mL with 10 mg L^{-1} initial concentration of As(V) (from a stock solution of 0.416 g of $Na_2HAsO_4.7H_2O$ in 1000 mL of distilled water) in agitation at 200 rpm and pH 7, and 3 mL of sample was taken from t = 0 to t = 24–36 h for remaining arsenic quantification. In the studies of As(V) adsorption isotherms, 0.14 g of the material was taken in a volume of 10 mL with 0.1–100 mg As(V) L^{-1} for 24 h, in agitation at 200 rpm, pH 7, and room temperature (~25 °C). After 24 h, the powder-form samples from the experiment were filtered, while the monoliths were removed from the solution. All the experiments of adsorption kinetics and adsorption isotherms were done in duplicate. The remaining and initial arsenic concentrations in the aqueous solutions were quantified by atomic absorption spectroscopy (ICE 3000 Thermo Scientific), with which the adsorption capacities for each material were calculated.

The experimental data obtained from adsorption kinetics were correlated by pseudo first order (PFO), pseudo second order (PSO), Internal Diffusion (ID) and Elovich models using the following equations:

$$q_{t(PFO)} = q_{te}(1 - e^{-K_1 t}) \quad (1)$$

$$q_{t(PSO)} = \frac{q_{te}^2 K_2 t}{1 + K_2 q_{te} t} \quad (2)$$

$$q_{t(ID)} = K_{ID} t^{\frac{1}{2}} + C_{ID} \quad (3)$$

$$q_{t(\text{Elovich})} = \frac{1}{\beta}\ln(\alpha\beta) + \frac{1}{\beta}\ln(t) \quad (4)$$

where q_t, in mg g^{-1}, is the adsorption capacity for each t, q_{te}, in mg g^{-1}, is the calculated adsorption capacity reached at equilibrium, t, in h, is the adsorption time corresponding to each sample, K_1, K_2 and K_{ID} are the constants associated with each model, in h^{-1}, g mg^{-1} h^{-1} and mg g^{-1} $h^{-0.5}$, respectively, C_{ID}, in mg g^{-1}, refers to the thickness of the boundary layer, and finally α, in mg g^{-1} h^{-1}, is the initial adsorption rate and β, g mg^{-1}, is related to the surface covered and the activation energy (Tran et al., 2017).

The Langmuir, Freundlich and SIPS models were used to fit the experimental isotherm, with the equations described below:

The Langmuir model is represented mathematically as:

$$q_{e(\text{Langmuir})} = \frac{q_{\max} K_L C_e}{1 + K_L C_e} \quad (5)$$

where q_e, in mg g^{-1}, is the amount of solute adsorbed in the adsorbent; C_e, in mg L^{-1}, is the existing equilibrium concentration of the solute in the solution, $q_{\max}$, in mg g^{-1}, is the amount of solute adsorbed on the solid when the monolayer has been formed (or maximum adsorption capacity of the solid), and K_L, in L mg^{-1}, is the Langmuir constant related to adsorption enthalpy (Murillo et al., 2015).

The Freundlich model can be expressed as:

$$q_{e(\text{Freundlich})} = K_F C_e^{\frac{1}{n}} \quad (6)$$

where K_F, in $L^{1/n}$ $mg^{1-1/n}$ g^{-1}, and n are characteristic constants of the model, whose values are a function of the type of adsorbate–adsorbent system and the temperature. The parameter n is considered a measure of the intensity of the adsorption (Tran et al., 2017).

The SIPS model is represented as:

$$q_{e(\text{SIPS})} = \frac{q_s K_s C_e^m}{1 + K_s C_e^m} \quad (7)$$

where K_S, in L^m mg^{-m}, corresponds to the adsorption affinity and m quantifies the heterogeneity of the adsorbent surface. This model describes monolayer adsorption at high concentration values, which is characteristic of the Langmuir model, and its behaviour is close to the Freundlich model at low concentration values.

In general, it can be said that when an adsorption isotherm is modelled closer to the Langmuir isotherm, the adsorption is restricted to a single layer, and the surface is energetically homogeneous. On the other hand, if the Freundlich model better represents the experimental isotherm, it is associated with multilayer adsorption on a heterogeneous surface. The SIPS model is an empirical equation involving parameters of both isotherms (Langmuir and Freundlich) and can describe the heterogeneity of the adsorbent surface (Tran et al., 2017).

Results and discussion

Improved monolith synthesis conditions and As(V) adsorption studies in water

As mentioned above in 'Materials and methods' section, previous studies were conducted to determine the optimal synthesis conditions that maximize the removal capacity of the monoliths, finding that for the CM with addition of bone meal the selected carbonization was in an inert atmosphere at 700 °C, this finding was consistent with the results reported in the literature (Rojas-Mayorga et al., 2016); and with the addition of powdered iron, the optimal calcination conditions were 600 °C in air. It was also decided to explore the possibility of combining both active phases in a monolith, a material composed of 25% iron powder, 50% bone meal, 20% bentonite clay and 5% carboxymethylcellulose. This mixture was subjected to 700 °C in N_2 to obtain the final monolith. The synthesized materials are shown in Figure 1.

Due to the fact that the synthesized materials are proposed in a 3D structure, chemical stability experiments were carried out in aqueous medium at high, low and neutral

pH, where it was found that all materials present high stability since they maintained their integrity and presented mass losses by leaching of less than 2%.

Additionally, tests were conducted to determine the PZC, with the results presented in Figure 2. The findings indicate that the monoliths exhibit minimal variation in PZC, regardless of their composition, with values ranging from 7.5 to 7.8. This suggests that at neutral pH, the monoliths carry a slight positive charge, which may enhance the adsorption of arsenate anions. However, studies on the effects of pH were not performed, as the focus of this research has been to develop the synthesized materials for conditions that more closely resemble real-world scenarios, thereby establishing a foundation for future scalability studies.

Table 4 and Figure 3 display the outcomes of the kinetic study with CM_Fe, CM_BC and CM_BC@Fe, including the calculated parameters for the kinetic models used and an arsenic concentration profile. Figure 3(a) shows the kinetics of the CM_Fe whose best fit of the kinetic equations was obtained with PFO model (see Table 4). It can be observed that it has slow kinetics and the adsorption system begins a pronounced increase in the As(V) adsorption at >6 h until reaching the equilibrium after 24 h. This may be since in the first place, arsenic anions find the OH-Al or OH-Si groups of clay edge sites. However, the Fe-O group is much more attractive and has a greater capacity for removal (Berrones & Lascano, 2009) but diffusion within the monolith is slow until such active sites are found.

Figure 3(b) shows the arsenic adsorption kinetics of the material CM_BC, which was a little faster and exceeded more than 60% of its adsorption capacity after 6 h. The model that best describes the kinetics of this material is the Elovich equation or PSO model, so the adsorption occurs with heterogeneous active sites and different activation energies. This result was somewhat expected because bone char presents a variety of surface groups with which As(V) interacts, such as carbonate or phosphate groups (Rojas-Mayorga et al., 2016).

Figure 3(c) shows the adsorption kinetics of As(V) on the composite CM, and it can be seen that the adsorption was faster compared to materials with the active phases separately since at less than 5 h of contact time were required to reach almost 80% of the removal capacity. Additionally, this system reached equilibrium before 4 h of contact time. This may be because the material possesses a large number of active sites for As(V), such as the hydroxyl groups of the clay edge sites, the carbonate or phosphate groups of BC or the Fe-O group from the powdered iron added to the material. The best fit was found with the PSO model, which did not differ significantly from the PFO model, suggesting that more information is needed to determine the mechanism or phenomenon that governs the As(V) adsorption on the composite material (Liu et al., 2024).

Finally, Figure 3(d) illustrates the arsenic concentration profile over time for the three ceramic monoliths (CMs) studied. It is evident that the composite not only achieves complete As(V) removal from the solution but also exhibits faster adsorption kinetics compared to the CMs with individual active phases. During the initial hours of contact, there is a marked decrease in the contaminant concentration, reaching 90% removal, followed by a slower reduction until equilibrium is attained.

Figure 4 shows the results obtained in the arsenic adsorption equilibrium experiments on the materials studied, where it can be evidenced that the composite material has the highest removal capacity than the materials with the active phases separately, which suggests that the combination of both raw materials presents a synergy on the final material properties, whereby iron and bone meal collaboratively enhance the dispersion and availability of active sites for arsenic adsorption, this combination may facilitate the formation of new adsorption sites or improve the accessibility of

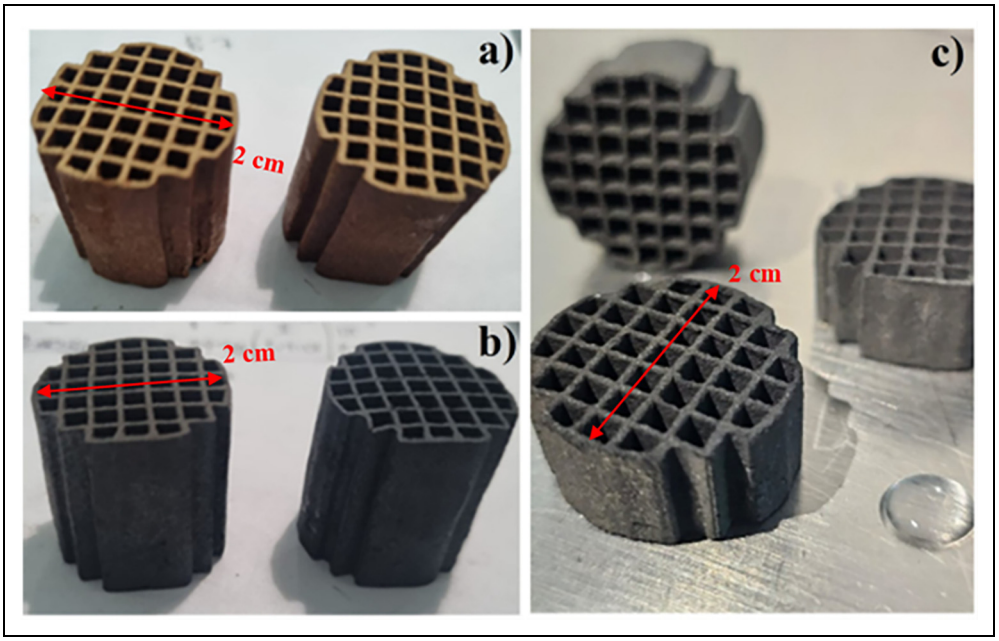

Figure 1. Ceramic monoliths. Samples: (a) CM_Fe, (b) CM_BC and (c) CM_BC@Fe. *The height of the CM varies between 1 and 2 cm as required.

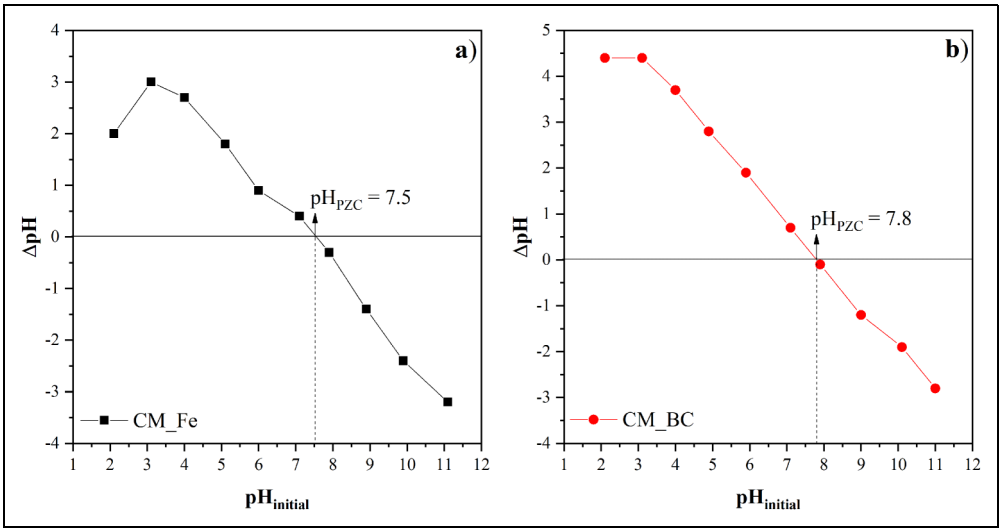

Figure 2. Point of zero charge of materials (a) CM_Fe and (b) CM_BC.

pre-existing ones. Additionally, the experimental isotherm obtained by the composite material was an L-type isotherm that says that the adsorbate has a great affinity with the adsorbent surface and that CM_BC@Fe material has a good performance at low and high concentrations of arsenic, reaching a maximum adsorption capacity of 8.0 mg As(V) g^{-1}.

Table 4. Kinetic data modelling for the adsorption of arsenic on ceramic monoliths.

Kinetic model	Parameter	CM_Fe	CM_BC	CM_BC@Fe
Intraparticle difusión	K_{ID} (mg g^{-1} $h^{-0.5}$)	0.024	0.066	1.105
	C_{ID} (mg g^{-1})	0.01	0.023	1.228
	R^2	0.958	0.953	0.856
Pseudo first order	q_e (mg g^{-1})	0.166	0.344	5.270
	K_1 (h^{-1})	0.086	0.179	0.672
	R^2	0.988	0.989	0.995
Pseudo second order	q_e (mg g^{-1})	0.206	0.406	5.824
	K_2 (g mg^{-1} h^{-1})	0.432	0.514	0.152
	R^2	0.964	0.995	0.997
Elovich	α (mg g^{-1} h^{-1})	0.115	0.292	15.94
	β (g mg^{-1})	33.78	13.93	0.999
	R^2	0.886	0.996	0.988

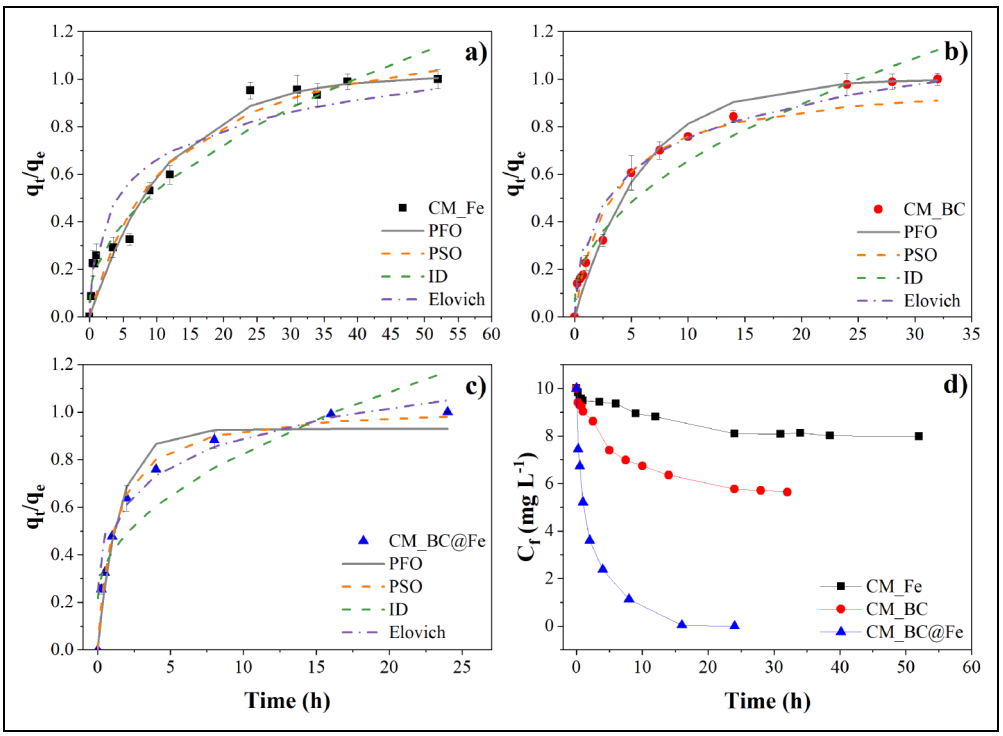

Figure 3. Kinetics for the As(V) adsorption on (a) CM_Fe (■), (b) CM_BC (●), (c) CM_BC@Fe (▲) and (d) arsenic concentration profile (m ≈ 6 g, V = 0.5 L and initial concentration ≈ 10 mg L^{-1}).

The values found for the different models of adsorption isotherms are presented in Table 5, where it can be evidenced that the SIPS model is the one that best represents the arsenic adsorption using tested materials, suggesting the heterogeneity of the adsorbent surface, which was consistent with their composition.

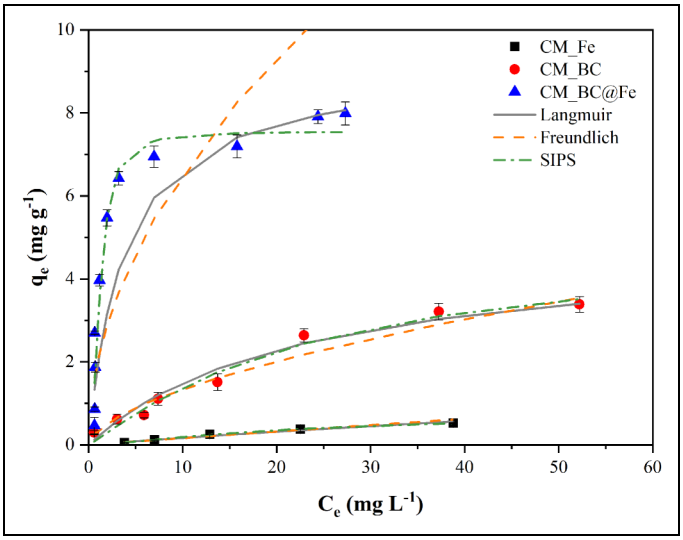

Figure 4. Isotherms of As(V) adsorption on CM_Fe (■), CM_BC (●) and CM_BC@Fe (▲).

Table 5. Isotherm data modelling for the adsorption of arsenic on ceramic monoliths.

Isotherm Model	Parameter	CM_Fe	CM_BC	CM_BC@Fe
Langmuir	q_{max} (mg g^{-1})	3.09	4.88	9.17
	K_L (L mg^{-1})	0.0057	0.044	0.266
	R^2	0.240	0.853	0.912
Freundlich	K_F (L$^{1/n}$ mg$^{1-1/n}$ g^{-1})	0.018	0.345	2.04
	n	1.03	1.70	1.97
	R^2	0.974	0.966	0.624
SIPS	q_S (mg g^{-1})	0.743	4.94	7.55
	K_S (L^m mg^{-m})	0.047	0.043	0.808
	m	1.43	1.12	2.12
	R^2	0.999	0.996	0.999

Physicochemistry of CMs and As(V) adsorption mechanisms

To be able to relate the performance of each material in the As(V) removal in an aqueous medium with the physicochemical properties of the synthesized monoliths, the raw materials and the CMs were characterized mineralogically, texturally, morphologically, chemically and mechanically, and the results are discussed below.

Figure 5 shows the diffractograms obtained for the raw materials (Figure 5(a)) and the monoliths (Figure 5(b)–(d)) with active bone meal and iron powder phases. In these diffractograms, it can be seen that the crystalline phases found in the monoliths are mostly the same as those present in the raw materials, as observed in Figures 4(b) to (d), highlighting the permanence of montmorillonite as the majority phase of bentonite clay, the permanence of hydroxyapatite and calcite in the bone char monolith, and mostly the magnetite phase in the iron monolith. Additionally, it can be observed that the intensity of the phase reflections present in the raw materials decreases significantly in the

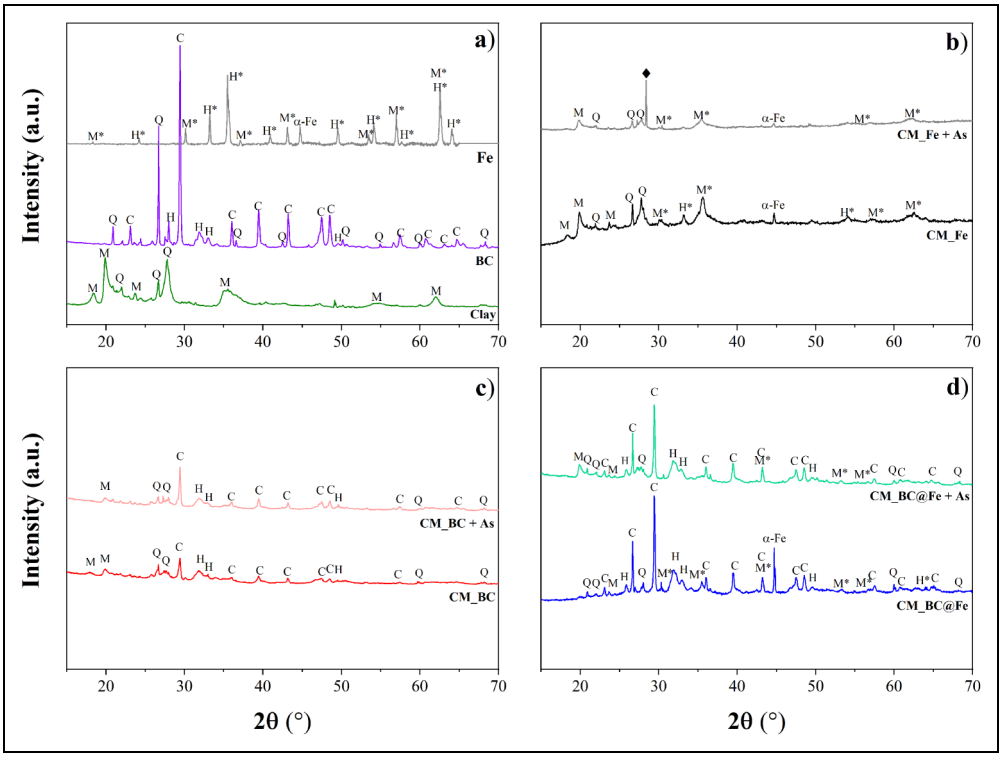

Figure 5. The X-ray diffraction (XRD) patterns of (a) raw materials, and CM before and after the arsenic adsorption test, (b) CM_Fe, (c) CM_BC and (d) CM_BC@Fe. Nomenclature: M: Montmorillonite, Q: Quartz, H: Hydroxyapatite, C: Calcite, M*: Magnetite, H*: Hematite, α-Fe: α-Iron.

ceramic monolith, which shows that these materials tend to lose crystallinity.

Figure 6(a) presents the FTIR spectra of raw materials, which contain two common regions of absorption bands. The stretching vibration of the OH groups corresponds to the signal at 3460 cm^{-1} (Mudzielwana et al., 2020; Rojas-Mayorga et al., 2013), while the IR band at 1638 cm^{-1} represents the H–O–H bending vibration of adsorbed water on the iron powder (Berrones & Lascano, 2009) and water molecules within the clay interlayers for the bentonite (Mudzielwana et al., 2020).

In montmorillonite clay, an absorption band is observed at 3630 cm^{-1} that can be related to the stretching of the O-H bonds (tension vibration). It indicates a significant amount of aluminum cations in the octahedral sheet of the clay (Roca Jalil et al., 2015). Si-O-Si bonds are assigned to 1041 cm^{-1} band, while the absorption bands at 525 and 468 cm^{-1} are due to Al–O–Si and Si–O–Si bending vibrations, respectively (Roca Jalil et al., 2015; Rojas-Mayorga et al., 2016). The absorption bands below 900 cm^{-1} are those in which the deformations of the bonds present in octahedral sheets appear, that is, 898 cm^{-1} (Al-Fe-OH) and 833 cm^{-1} (Al-OH-Mg) (Roca Jalil et al., 2015).

Figure 6(a) also shows the IR spectrum with the absorption bands of the organic and inorganic phases corresponding to the structure of the bone char: C = O (1625 cm^{-1}), C = C (1450 cm^{-1}), PO_4^{3-} asymmetric stretching vibration mode (1014 cm^{-1}), P–O bending vibration mode (960 and 605 cm^{-1}), CO_3^{2-} (1445 and 870 cm^{-1}) and Ca-O bond (565 cm^{-1}) (Rojas-Mayorga et al., 2016). For the IR spectrum corresponding to Fe powder, the

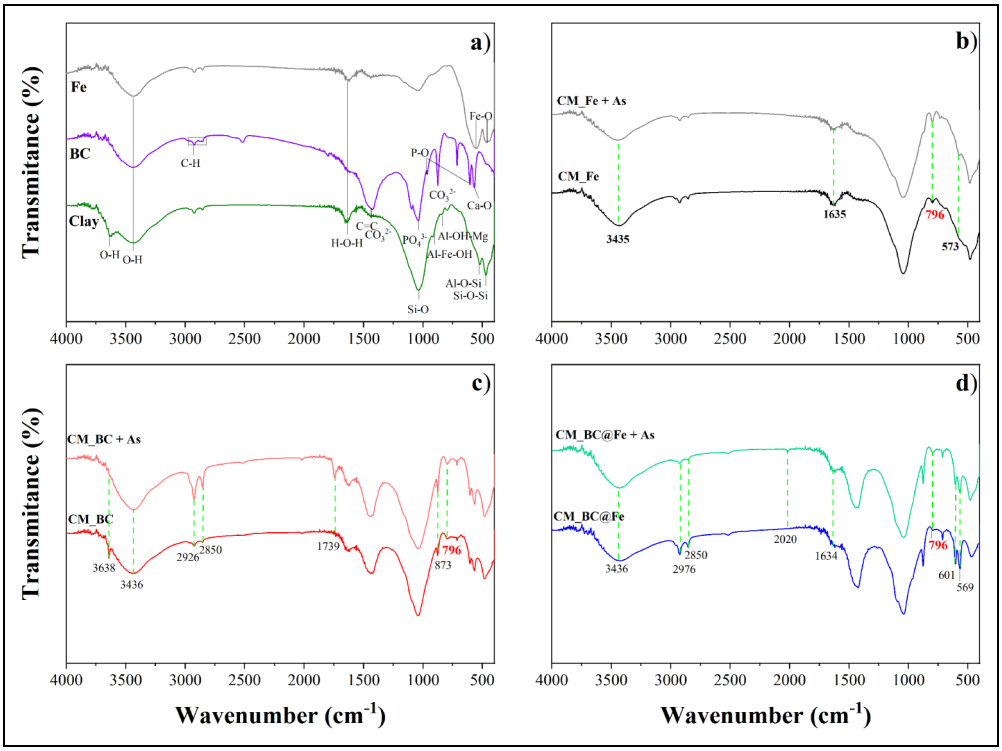

Figure 6. Fourier Transform Infrared Spectroscopy (FTIR) spectra of (a) raw materials and CM before and after the arsenic adsorption test, (b) CM_Fe, (c) CM_BC and (d) CM_BC@Fe.

characteristic absorption bands of the Fe-O bond can be observed at 550 and 443 cm^{-1} (Benhammada et al., 2020; Berrones & Lascano, 2009; Mahmoud & Hamid Mahmoud, 2017; Xu et al., 2011; Yadav et al., 2020).

Figure 6(b) to (d) shows the IR spectra of the CMs with the active phases and the composite CM, before and after arsenic adsorption testing, and some changes in the intensities of the bands related to the OH groups can be observed, suggesting an interaction between the hydroxyl groups and the arsenic species (Rojas-Mayorga et al., 2016). Additionally, an absorption band can be observed at 796 cm^{-1} in all material spectra after adsorption experiments, and this can be assigned as the symmetric tension vibration of the As-(OFe) bond, indicating the presence of inner-sphere bidentate unprotonated arsenate surface complexes (Brechbühl et al., 2012).

Figure 7 shows the micrographs of the ceramic monoliths obtained. In particular, Figure 7(a) and (b) shows the micrographs of the CM_Fe where a rough and non-porous surface can be observed, see Figure 7(a). However, the nano husk or self-oriented flower morphology specific to iron oxides (Sayed & Polshettiwar, 2015) is observed (highlighted in the red boxes) at higher magnification. Figure 7(c) and (d) shows the micrographs of the CM_BC, which presents a marked roughness with a more porous and irregular surface. A similar morphology can also be seen in Figure 7(e) and (f) of the micrographs of the composite material, where the morphology of the iron oxides that occur on the surface of the material can be identified at higher magnification.

Figure 8(a) displays the Hg intrusion-extrusion curves obtained from Fe ceramic

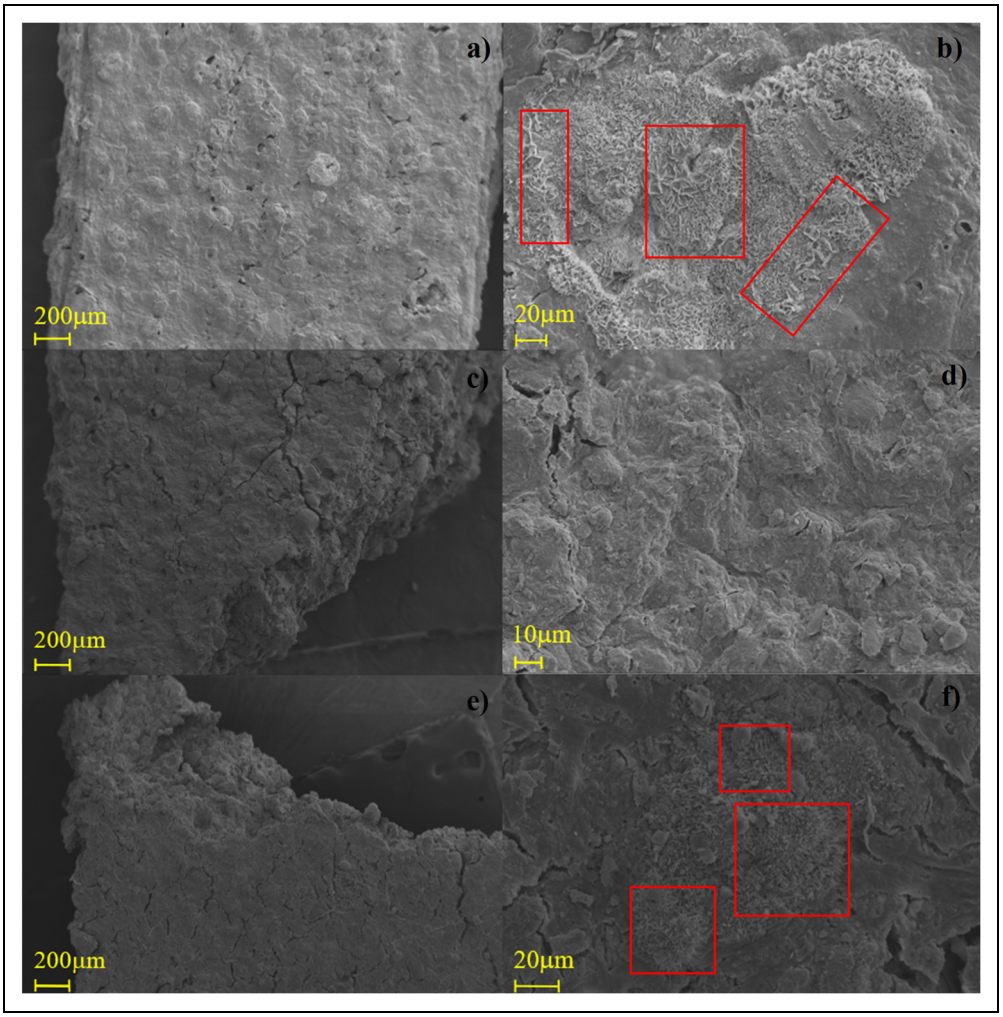

Figure 7. Micrographs of ceramic monoliths: (a–b) CM_Fe, (c–d) CM_BC and (e–f) CM_BC@Fe.

materials, BC, and the material containing both phases. In the curve of the Fe material (■), it is observed that, up to a pressure of 1 MPa, there is a very small increase in the accumulated volume, which is associated with the low quantity of large macropores. In contrast, the curves of CM_BC and CM_BC@Fe (● and ▲, respectively) show a similar increase in the accumulated volume until reaching approximately 0.1 MPa of pressure, where the composite material exhibits a pronounced increase in this region, indicating the presence of a group of well-defined large macropores. Subsequently, the curves of all materials (CM_Fe, CM_BC and CM_BC@Fe) exhibit two stages of increase in the accumulated volume, one up to 40 MPa, and the last stage with a more pronounced increase up to 200 MPa, indicating that these materials present mesopores, as can be seen in Figure 8(b) and (c). In agreement with the discussion, it can be observed that the pore size distribution of all materials presents large macropores with a modal size of 9 µm (primarily CM_BC@Fe) and mesopores with a modal size between 10 and 20 nm.

The textural properties of the ceramic monoliths are presented in Table 6 where, as

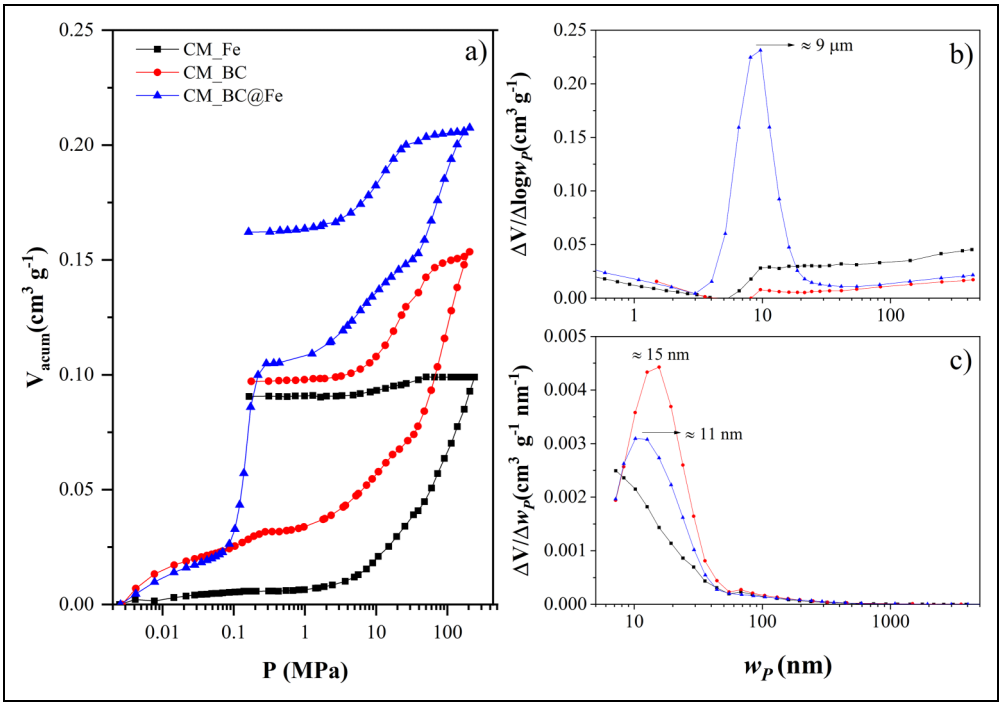

Figure 8. (a) Intrusion-extrusion curves of Hg of CMs, (b) Size distribution of large pores and (c) Size distribution of small pores, obtained with Hg Porosimetry. Samples: CM_Fe (■), CM_BC (●) and CM_BC@Fe (▲).

Table 6. Textural properties of ceramic monoliths.

	Mercury porosimetry				
CM	S_{Hg} (m^2 g^{-1})	V_{TP-Hg} (cm^3 g^{-1})	Porosity (%)	ρ_{bulk} (g cm^{-3})	$\rho_{skeletal}$ (g cm^{-3})
CM_Fe	23.7	0.10	21.9	2.1	2.7
CM_BC	25.7	0.15	22.2	1.4	1.9
CM_BC@Fe	17.2	0.21	31.1	1.5	2.2

expected, the composite material presents greater porosity and greater total pore volume, due to the presence of macroporosity, but the specific surface area decreased compared to the CMs of Fe and BC alone.

It is important to highlight that the surface chemistry of the adsorbent materials plays a relevant role in the arsenic removal from aqueous medium. However, textural properties of ceramic monoliths are also of vital importance, as they directly affect the diffusion of the adsorbate on the material. Therefore, it can be proposed that there is not only a synergy in the active phases for the CM_BC@Fe but also the presence of macro and mesoporosity in the monolith promotes the phenomenon of adsorption of As(V) on the material, so it presents greater capacities compared to CMs with active phases separately.

Figure 9 shows the stress vs. strain graphs for ceramic monoliths, where the CM_Fe has

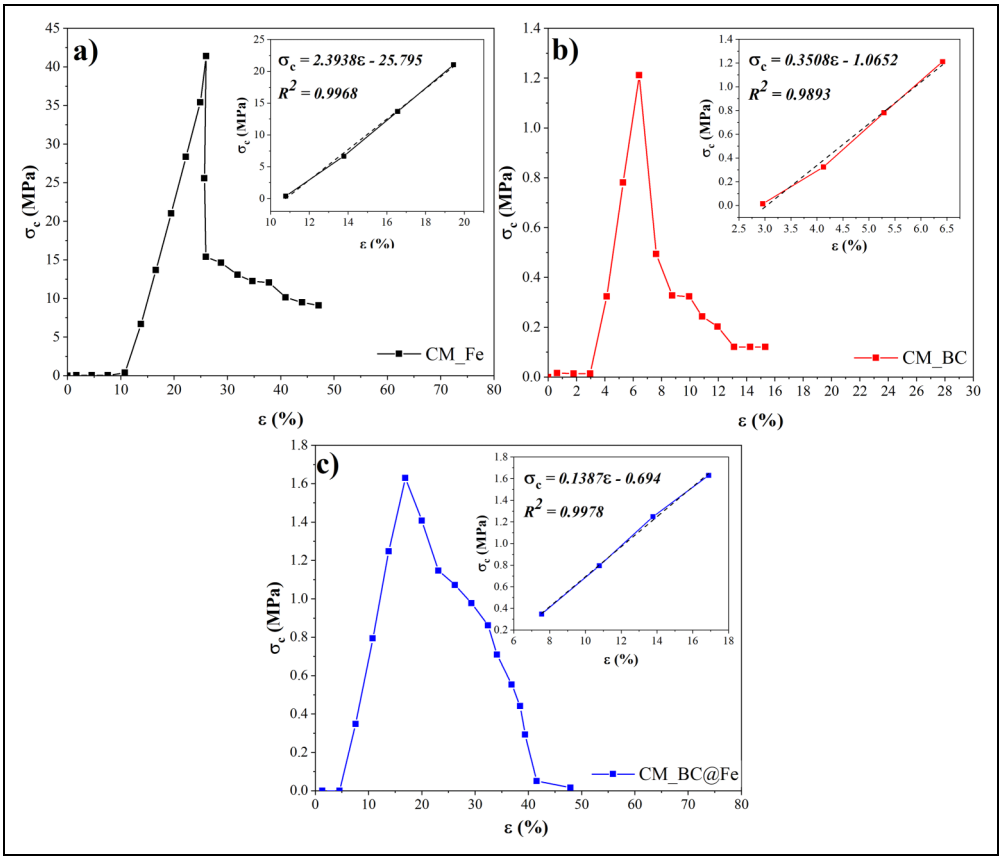

Figure 9. Compressive stress vs strain (σ_c vs. ϵ) plots of CMs: (a) CM_Fe (■), (b) CM_BC (●) and (c) CM_BC@Fe (▲).

Table 7. Mechanical properties of CMs obtained by axial compression tests.

	Maximum load	Compressive stress*	Strain*	Young's modulus
CM	*(N)*	*σ_c (MPa)*	*ϵ (%)*	*E (MPa)*
CM_Fe	9100	41.4	26.1	2.39
CM_BC	266	1.2	6.4	0.35
CM_BC@Fe	427	1.6	16.8	0.14

*At the point of maximum load and moment of rupture.

excellent mechanical properties, reaching compressive stress (>41 MPa) significantly higher than that reported for commercial cordierite, alumina and quartz (Cybulski and Moulijn, 1994; García-Carvajal, 2019; Khomenko et al., 2024) materials, and compared to other reported ceramic clay and zeolite monoliths (García-Carvajal et al., 2022). It can be seen in Figure 9(b) and (c) that the compressive stress values are significantly lower, but that the composite material has better mechanical properties than the material based only on BC (see Table 7), thus also highlighting the positive influence of the addition of Fe on the CM.

Table 8. Conformal materials reported for arsenic removal.

Adsorbents	Initial concentration (mg L^{-1})	Adsorption capacity – As(V) (mg g^{-1})	pH	Reference
Ceramic alumina membrane with micro and nanoparticles of Fe	1	0.496	3.5	Zaspalis et al. (2007)
Iron mixed ceramic pellet	2.5–20	4.5	7	Shafiquzzam et al. (2013)
Concrete/maghemite nanocomposite	0.1–1300	9.3	3–7	Hernández-Flores et al. (2018)
Reactive ceramic pellet with iron	10–100	0.041	3	Rha et al. (2019)
Hierarchical zeolite LTA monolith Yang et al. (2020)	1–100	5.11	1–12	
Granular chitosan–titanium adsorbent	0.1–10	8.1	8	Xu et al. (2011)
MIL-100(Fe) – chitosan beads Joseph et al. (2024)	1–100	60	3–11	
Iron/bone char ceramic monolith - CM_BC@Fe	0.1–100	8.0	7	This study
Bentonite clay (powder)	10	0.001	7	This study
Bone char (powder)	10	0.54	7	This study
Iron powder	10	0.71	7	This study

Additionally, it should be noted that all the synthesized monoliths have compressive stress values higher than those required for materials. These materials are typically required to withstand pressures greater than 0.48–0.68 MPa (Crittenden, 2005), making these materials mechanically viable for use in adsorption processes in continuous systems.

Table 8 shows the As(V) removal capacities of several conformal adsorbent materials reported in the literature, where it can be observed that the composite monolith synthesized in this study exhibits capacities comparable to those reported, highlighting the low cost of the raw materials, as well as the excellent mechanical properties and defined porosity of the synthesized material.

Finally, as an initial cost assessment, an analysis revealed that the composite monolith is the most expensive material synthesized in this study, with a total cost of \$5 USD kg^{-1}, comprising \$3 USD for raw materials and \$2 USD for operating expenses. According to authors (GadelHak et al., 2023), materials can be classified as low cost if they do not exceed \$1 USD kg^{-1}, intermediate cost if they fall between \$3 and \$6 USD kg^{-1} and high cost if they range from \$15 to \$20 USD kg^{-1}. Therefore, while the monoliths were synthesized from low-cost raw materials, their resulting cost falls into the intermediate category.

It is important to note that the composite features two active phases and is produced in a three-dimensional shape that facilitates handling and operation during adsorption processes. Additionally, the cost analysis was conducted at the laboratory scale, suggesting that scaling up production could lead to a reduction in the overall cost of these materials.

Conclusions

The study was conducted to optimize the adsorption capacity of monoliths for arsenic(V) removal by exploring various synthesis conditions. These monoliths demonstrated exceptional mechanical properties and well-defined porosity, rendering them suitable

for applications in continuous water treatment systems. Notably, adsorption capacities of 0.56, 3.4 and 8.0 mg g^{-1} were obtained for monoliths incorporating hematite/magnetite, bone char and a combination of both materials. The CM_Fe presented mechanical properties comparable to commercial monoliths and it is suggested that iron may provide structural reinforcement by acting within the ceramic matrix to enhance cohesion among the material's particles. This reinforcement could improve the monolith's capacity to withstand compressive forces.

Synergistic effects were observed upon combining both active phases, leading to faster kinetics and significantly higher removal capacities than individual materials. The formation of inner-sphere bidentate unprotonated arsenate surface complexes played a relevant role in the arsenic adsorption mechanism.

In conclusion, synthesizing clay-based monoliths incorporating waste-derived active phases, such as powdered iron and bone meal, represents a promising advancement in arsenic(V) removal technology. These findings underscore the potential of utilizing waste-derived materials in clay-based monoliths for effective arsenic removal, with significant implications for environmental remediation efforts and sustainable waste management practices.

Lastly, future research could explore experiments aimed at regenerating the synthesized monoliths using saline solutions that exhibit an affinity for arsenic, or by employing thermal desorption techniques. These approaches may enhance the competitiveness of the ceramic monoliths (CMs) as adsorbents for the As(V) removal from aqueous media.

Data availability statement

All data generated or analyzed during this study are included in this published article.

Declaration of conflicting interests

The author(s) declared no potential conflicts of interest concerning the research, authorship, and/or publication of this article.

Ethical approval

We confirm that this work is original and has not been published elsewhere nor is it currently under consideration for publication elsewhere.

Funding

The author(s) disclosed receipt of the following financial support for the research, authorship, and/or publication of this article: This work was financially supported by CONICET (Argentina) with a Doctoral scholarship for C. G-C, Universidad Nacional de San Luis; and by Mexican Agency for International Development Cooperation with an excellence grant awarded to C. G-C (2022).

ORCID iDs

Jhonny Villarroel-Rocha https://orcid.org/0000-0002-4323-3360
Karim Sapag https://orcid.org/0000-0003-2266-1363

References

Alka S, Shahir S, Ibrahim N, et al. (2021) Arsenic removal technologies and future trends: A mini review. *Journal of Cleaner Production* 278: 123805.

Alkurdi SSA, Al-Juboori RA, Bundschuh J, et al. (2021) Inorganic arsenic species removal from water using bone char: A detailed study on adsorption kinetic and isotherm models using error functions analysis. *Journal of Hazardous Materials* 405: 124112.

Altowayti WAH, Othman N, Shahir S, et al. (2022) Removal of arsenic from wastewater by using different technologies and adsorbents: A review. *International Journal of Environmental Science and Technology* 19(9): 9243–9266.

Avila P, Montes M and Miró E (2005) Monolithic reactors for environmental applications A review on preparation technologies. *Chemical Engineering Journal* 109: 11–36.

Baigorria E, Cano L and Alvarez VA (2021) Nanoclays as eco-friendly adsorbents of arsenic for water purification. In: Kharissova OV, Torres-Martínez LM and Kharisov BI (eds) *Handbook of Nanomaterials and Nanocomposites for Energy and Environmental Applications*. Switzerland:

Springer International Publishing, 455–470. https://doi.org/10.1007/978-3-030-36268-3_61.

Benhammada A, Trache D, Kesraoui M, et al. (2020) Hydrothermal synthesis of hematite nanoparticles decorated on carbon mesospheres and their synergetic action on the thermal decomposition of nitrocellulose. *Nanomaterials* 10(5): 68.

Berrones MA and Lascano L (2009) Síntesis de nanopartículas de hematita por el método de precipitación controlada. *Revista Politécnica* 30(1): 91–99.

Brechbühl Y, Christl I, Elzinga EJ, et al. (2012) Competitive sorption of carbonate and arsenic to hematite: Combined ATR-FTIR and batch experiments. *Journal of Colloid and Interface Science* 377(1): 313–321.

Brunson LR and Sabatini DA (2009) An evaluation of fish bone char as an appropriate arsenic and fluoride removal technology for emerging regions. *Environmental Engineering Science* 26(12): 1777–1784.

Chen Y-N, Chai L-Y and Shu Y-D (2008) Study of arsenic(V) adsorption on bone char from aqueous solution. *Journal of Hazardous Materials* 160(1): 168–172.

Costa FCR, Moreira VR, Guimarães RN, et al. (2024) Arsenic in natural waters of Latin-American countries: Occurrence, risk assessment, low-cost methods, and technologies for remediation. *Process Safety and Environmental Protection* 184: 116–128.

Crittenden JC (2005) *Water Treatment: Principles and Design / MWH ; Revised by John C. Crittenden … [et al.]*, 2nd ed. Hoboken, New Jersey: J. Wiley.

Cybulski A and Moulijn JA (1994) Monoliths in heterogeneous catalysis. *Catalysis Reviews-Science and Engineering - CATAL REV-SCI ENG* 36: 179–270.

Farrell J and Chaudhary BK (2013) Understanding arsenate reaction kinetics with ferric hydroxides. *Environmental Science and Technology* 47(15): 8342–8347.

GadelHak Y, El-Azazy M, Shibl MF, et al. (2023) Cost estimation of synthesis and utilization of nano-adsorbents on the laboratory and industrial scales: A detailed review. *Science of The Total Environment* 875: 162629.

García-Carvajal C, 2019. *Desarrollo de materiales cerámicos conformados mediante la técnica de extrusión y peletización*. Magister Thesis. Universidad Nacional de San Luis, Argentina.

García-Carvajal C, Villarroel-Rocha J, Curvale D, et al. (2019) Arsenic (V) removal from aqueous solutions using natural clay ceramic monoliths. *Chemical Engineering Communications* 206(11): 1440 1451.

García-Carvajal C, Villarroel-Rocha J, de Souza VC, et al. (2022) Development of ceramic honeycomb monolith from natural zeolite tested as adsorbent to remove methylene blue in aqueous media. *Environmental Science and Pollution Research International* 29(53): 79890–79902.

Gong S, Yang J, Zhou W, et al. (2023) Fe-containing materials for inorganic/organic arsenic removal from water: A review of current status and future prospects. *Journal of Cleaner Production* 428: 139533.

Gu Z, Deng B and Yang J (2007) Synthesis and evaluation of iron-containing ordered mesoporous carbon (FeOMC) for arsenic adsorption. *Microporous and Mesoporous Materials* 102: 265–273.

Hao L, Liu M, Wang N, et al. (2018) A critical review on arsenic removal from water using iron-based adsorbents. *RSC Advances* 8(69): 39545–39560.

Hernández-Flores H, Pariona N, Herrera-Trejo M, et al. (2018) Concrete/maghemite nanocomposites as novel adsorbents for arsenic removal. *Journal of Molecular Structure* 1171: 9–16.

Huo L, Zeng X, Su S, et al. (2017) Enhanced removal of as (V) from aqueous solution using modified hydrous ferric oxide nanoparticles. *Scientific Reports* 7(1): 40765.

Joseph J, Väisänen A, Patil AB, et al. (2024) The effect of synthesis conditions on the *in situ* grown MIL-100(fe)-chitosan beads: Interplay between structural properties and arsenic adsorption. *Journal of Hazardous Materials* 463: 132893.

Khomenko O, Zaichuk A and Amelina A (2024) Low-temperature cordierite ceramics with porous structure for thermal shock resistance products. *Open Ceramics* 17: 100520.

Ladeira ACQ and Ciminelli VSTVST (2004) Adsorption and desorption of arsenic on an

oxisol and its constituents. *Water Research* 38(8): 2087–2094.

Lafferty BJ and Loeppert RH (2005) Methyl arsenic adsorption and desorption behavior on iron oxides. *Environmental Science & Technology* 39(7): 2120–2127.

Litter M. I. (2010). Possible treatments for arsenic removal in Latin American waters for human consumption. *Environmental Pollution* 158: 1105–1118. https://www.academia.edu/14115994/Possible_treatments_for_arsenic_removal_in_Latin_American_waters_for_human_consumption

Liu J, Huang X, Liu J, et al. (2014) Adsorption of arsenic(V) on bone char: Batch, column and modeling studies. *Environmental Earth Sciences* 72(6): 2081–2090.

Liu Y, Chen L, Yang L, et al. (2024) Porous framework materials for energy & environment relevant applications: A systematic review. *Green Energy & Environment* 9(2): 217–310.

Mahmoud ZH and Hamid Mahmoud Z (2017) The magnetic properties of alpha phase for iron oxide nps that prepared from its salt by novel photolysis method. *Journal of Chemical and Pharmaceutical Research* 9(8): 29–33.

Mohanty D (2017) Conventional as well as emerging arsenic removal technologies—A critical review. *Water, Air, and Soil Pollution* 228(10): 381.

Mohapatra D, Mishra D, Chaudhury GR, et al. (2007) Arsenic adsorption mechanism on clay minerals and its dependence on temperature. *Korean Journal of Chemical Engineering* 24(3): 426–430.

Mudzielwana R, Gitari MW and Ndungu P (2020) Enhanced As(III) and As(V) adsorption from aqueous solution by a clay based hybrid sorbent. *Frontiers in Chemistry* 7: 913.

Mukhopadhyay R, Sarkar B, Barman A, et al. (2021) Arsenic adsorption on modified clay minerals in contaminated soil and water: Impact of pH and competitive anions. *CLEAN – Soil, Air, Water* 49(4): 2000259.

Murillo CA, Gomez OA, Ortiz Cancino OP, et al. (2015) Aplicación de modelos para la generación de la isoterma de adsorción de metano en una muestra de shale y su impacto en el cálculo de reservas. *Fuentes: El Reventón Energético* 13(2): 131–140.

Mustafa S, Dilara B, Nargis K, et al. (2002) Surface properties of the mixed oxides of iron and silica. *Colloids and Surfaces A: Physicochemical and Engineering Aspects* 205(3): 273–282.

Rha S, Gong YS and Jo HY (2019) Reactive ceramic pellets incorporated iron for removing as(III), as(V), and cr(VI) from aqueous solutions. *Desalination and Water Treatment* 158: 174–186.

Roca Jalil ME, Baschini M and Sapag K (2015) Influence of pH and antibiotic solubility on the removal of ciprofloxacin from aqueous media using montmorillonite. *Applied Clay Science* 114: 69–76.

Rojas-Mayorga CK, Bonilla-Petriciolet A, Aguayo-Villarreal IA, et al. (2013) Optimization of pyrolysis conditions and adsorption properties of bone char for fluoride removal from water. *Journal of Analytical and Applied Pyrolysis* 104: 10–18.

Rojas-Mayorga CK, Mendoza-Castillo DI, Bonilla-Petriciolet A, et al. (2016) Tailoring the adsorption behavior of bone char for heavy metal removal from aqueous solution. *Adsorption Science and Technology* 34(6): 368–387.

Sayed FN and Polshettiwar V (2015) Facile and sustainable synthesis of shaped iron oxide nanoparticles: effect of iron precursor salts on the shapes of iron oxides. *Scientific Reports* 5: 9733.

Shafiquzzam M, Hasan MM and Nakajima J (2013) Iron mixed ceramic pellet for arsenic removal from groundwater. *Environmental Engineering Research* 18(3): 163–168.

Sharma PK, Kumar R, Singh RK, et al. (2022) Review on arsenic removal using biochar-based materials. *Groundwater for Sustainable Development* 17: 100740.

Singh P, Borthakur A, Singh R, et al. (2021) A critical review on the research trends and emerging technologies for arsenic decontamination from water. *Groundwater for Sustainable Development* 14: 100607.

Sneddon IR, Garelick H and Valsami-Jones E (2005) An investigation into arsenic(V) removal from aqueous solutions by hydroxylapatite and bonechar. *Mineralogical Magazine* 69(5): 769–780.

Srivastav AL, Pham TD, Izah SC, et al. (2022) Biochar adsorbents for arsenic removal from water environment: A review. *Bulletin of*

Environmental Contamination and Toxicology 108(4): 616–628.

Sylvester P, Westerhoff P, Möller T, et al. (2007) A hybrid sorbent utilizing nanoparticles of hydrous iron oxide for arsenic removal from drinking water. *Environmental Engineering Science* 24(1): 104–112.

Te B, Wichitsathian B and Yossapol C (2017) Adsorptive behavior of low-cost modified natural clay adsorbents for arsenate removal from water. *International Journal of GEOMATE* 12(33): 1–7.

Tran HN, You SJ, Hosseini-Bandegharaei A, et al. (2017) Mistakes and inconsistencies regarding adsorption of contaminants from aqueous solutions: A critical review. *Water Research* 120: 88–116.

Villarroel-Rocha J (2012) *Desarrollo de adsorbentes basados en arcillas y fosfatos naturales para la remoción de iones metálicos presentes en aguas*. San Luis, Argentina: Universidad Nacional de San Luis.

Weerasundara L, Ok Y-S and Bundschuh J (2021) Selective removal of arsenic in water: A critical review. *Environmental Pollution* 268: 115668.

Xu Y, Yang S, Zhang G, et al. (2011) Uniform hematite α-Fe2O3 nanoparticles: Morphology, size-controlled hydrothermal synthesis and formation mechanism. *Materials Letters* 65(12): 1911–1914.

Yadav VK, Ali D, Khan SH, et al. (2020) Synthesis and characterization of amorphous iron oxide nanoparticles by the sonochemical method and their application for the remediation of heavy metals from wastewater. *Nanomaterials* 10(8): 1551.

Yang X, Yan B, Liu Y, et al. (2020) Gamma-FeOOH based hierarchically porous zeolite monoliths for as(V) removal: Characterisation, adsorption and response surface methodology. *Microporous and Mesoporous Materials* 308: 110518.

Zaspalis V, Pagana A and Sklari S (2007) Arsenic removal from contaminated water by iron oxide sorbents and porous ceramic membranes. *Desalination* 217(1): 167–180.

Zhu H, Jia Y, Wu X, et al. (2009) Removal of arsenic from water by supported nano zero-valent iron on activated carbon. *Journal of Hazardous Materials* 172(2–3): 1591–1596.